Theoretical Study on Reaction Mechanism of the Cyanogen Radical with Nitrogen Dioxide

Jia-xu Zhang, Ze-sheng Li,* Jing-yao Liu, and Chia-chung Sun

Institute of Theoretical Chemistry, State Key Laboratory of Theoretical and Computational Chemistry, Jilin University, Changchun 130023, People's Republic of China

Received: July 23, 2005; In Final Form: September 21, 2005

The complex singlet potential energy surface for the reaction of CN with NO_2, including 9 minimum isomers and 10 transition states, is explored computationally using a coupled cluster method and a density functional method. The most favorable association of CN with NO_2 was found to be a barrierless carbon-to-nitrogen approach process forming an energy-rich adduct **a** ($NCNO_2$) followed by C−N bond rupture along with C−O bond formation to give $\mathbf{b}_1$ (*trans*-NCONO), which can easily convert to $\mathbf{b}_2$ (*cis*-NCONO). Our results show that the product $\mathbf{P}_1$ (NCO + NO) is the major product, while the product $\mathbf{P}_2$ (CNO + NO) is a minor product. The other products may be of significance only at high temperatures. Product $\mathbf{P}_1$ (NCO + NO) can be obtained through path 1 $\mathbf{P}_1$: $\mathbf{R} \rightarrow \mathbf{a} \rightarrow \mathbf{b}_1$ ($\mathbf{b}_2$) $\rightarrow \mathbf{P}_1$ (NCO + NO), whereas the product $\mathbf{P}_2$ (CNO + NO) can be formed through path $\mathbf{P}_2$: $\mathbf{R} \rightarrow \mathbf{a} \rightarrow \mathbf{b}_1 \rightarrow \mathbf{b}_2 \rightarrow \mathbf{c}_1$ ($\mathbf{c}_2$) $\rightarrow \mathbf{P}_2$ (CNO + NO). Because the intermediates and transition states involved in the above two channels are all lower than the reactants in energy, the CN + NO_2 reaction is expected to be rapid, as is confirmed by experiment. Therefore, it may be suggested as an efficient NO_2-reduction strategy. These calculations indicate that the title reaction proceeds mostly through singlet pathways and less go through triplet pathways. The present results can lead us to understand deeply the mechanism of the title reaction and can be helpful for understanding NO_2-combustion chemistry.

1. Introduction

The cyanogen radical CN is an important combustion species, particularly for nitrogen-containing fuels,[1−4] including nitramine energetic materials. In the combustion of nitramines such as RDX (hexahydro-1,3,5-trinitro-1,3,5-triazine), CN radical has been shown to be involved in the primary and secondary flame zones.[5] Extensive attention has been paid to the kinetics and mechanisms of CN reactions with various reagents of interest in planetary atmospheric chemistry[6] as well as in combustion chemistry.[7−10] The reaction of CN radical with NO_x ($x = 1, 2$) is not only relevant to the nitrogen chemistry of hydrocarbon combustion[11,12] but also very important in the combustion chemistry of nitramines, such as RDX and HMX.[13,14] On the other hand, it is known that nitrogen oxides (NO_x, $x = 1, 2$) are among the major atmospheric pollutants released by combustion processes. To minimize the harmful effects before their release into the atmosphere, one effective way is to reduce them by the reburning of combustion products.[15−20] The reactions of CN with NO_x may then provide an effective means for purging of the NO_x formed in combustion processes. Hence, reliable information on the kinetics of these CN reactions is of importance for the modeling of NO_x-combustion processes.

The reactions of some radicals (CH_3, CCO, and HCCO) with NO_2 have already been the subject of experimental and theoretical investigations.[21−26] A kinetic study of the reaction CN + NO_2 was also performed by Wang et al. using the two-laser pump−probe technique at temperatures between 297 and 740 K over a broad range of pressure.[7] The CN + NO_2 reaction was found to be pressure-independent, and the measured bimolecular rate constant can be represented by $k = 10^{-10.40\pm0.12}$ exp[(186 ± 23)/*T*] cm^3 $molecule^{-1}$ s^{-1}. At 298 K, the obtained value of the rate constant was (8.09 ± 0.17) × 10^{-11} cm^3 $molecule^{-1}$ s^{-1}, which indicates that the reaction of CN with NO_2 is very fast and may play an important role in the NO_2-combustion chemistry. However, there is a lack of information on product channels, product identification, and product distributions, although this information may be important in the NO_2-involved sequential chain processes. Wang et al.[7] proposed that the CN + NO_2 reaction occurs by simple abstraction mechanism, leading to species NCO and NO. However, the mechanism proposed by Wang et al. awaits further testing. In fact, our results show that the most favorable product NCO + NO is formed through complicated association, isomerization, and dissociation processes. Moreover, simply from the thermodynamic data, there are many other exothermic channels such as N_2 + CO_2 (−208.4 kcal/mol), N_2O + CO (−121.3 kcal/mol), and CNO + NO (−0.8 kcal/mol) for the title reaction.[27−29] In view of the potential importance and the rather limited experimental information, a careful theoretical study of the potential energy surface for this reaction is desirable. The main objectives of the present article are to (1) determine the various isomerization and dissociation channels on the $NCNO_2$ PES, (2) investigate the possible products of the title reaction to assist in further experiment identification, and (3) give a deep insight into the mechanism of cyanogen-NO_2-combustion reaction.

2. Computational Methods

All calculations are carried out using the GAUSSIAN98 program packages.[30] The geometries of all the reactants, products, intermediates, and transition states are optimized using the hybrid density functional B3LYP[31] method (the Becke's three-parameter hybrid functional with the nonlocal correlation functional of Lee−Yang−Parr) with 6-311G(d,p)[32−34] basis set. The stationary nature of structures is confirmed by harmonic vibrational frequency calculations; i.e., equilibrium species

* Corresponding author. Fax: +86-431-8498026. E-mail: Zeshengli@mail.jlu.edu.cn.

10.1021/jp054069a CCC: $30.25
Published on Web 10/22/2005

TABLE 1: Electronic States and Harmonic Vibrational Frequencies (cm^{-1}) of the Stationary Points at the B3LYP/6-311G(d,p) Level[a]

species	state	frequencies
CN	$^2\Sigma$	2152
		2069[b]
NO_2	$^2A'$	767, 1399, 1707
		750, 1318, 1618[c]
NO	$^2\Pi$	1988
		1904[c]
NCO	$^2\Pi$	504, 586, 1299, 1999
		534, 626, 1275, 1921[c]
CNO	$^2\Pi$	321, 417, 1202, 1934
N_2O	$^1\Sigma$	608, 608, 1336, 2358
		589,1287, 2224[c]
N_2	$^1\Sigma_g$	2448
		2359[b]
CO_2	$^1\Sigma_g$	667, 667, 1375, 2436
		667,1333, 2349[b]
CO	$^1\Sigma$	2220
		2170[c]
a	$^1A_1$	212(7), 278(18), 570(1), 628(0), 759(8), 908(58), 1349(147), 1645(313), 2337(15)
$\mathbf{b}_1$	$^1A'$	126(1), 161(5), 334(89), 520(9), 550(10), 721(113), 1142(39), 2028(776), 2279(52)
$\mathbf{b}_2$	$^1A'$	114(2), 234(0), 351(62) 541(45), 571(10), 704(1), 1172(27), 2034(512), 2237(48)
$\mathbf{c}_1$	$^1A'$	131(3), 266(0), 383(49), 420(1), 424(50), 735(17), 1054(26), 1983(442), 2095(24)
$\mathbf{c}_2$	$^1A'$	143(1), 147(2), 345(89), 363(0), 391(4), 740(158), 1038(18), 1991(679), 2140(44)
d	$^1A_1$	59(1), 109(0), 502(54), 621(8), 760(24), 839(224), 1301(288), 1737(393), 2110(369)
$\mathbf{e}_1$	$^1A'$	118(0), 168(1), 391(276), 628(24), 655(25), 765(154), 1332(112), 1785(715), 2279(997)
$\mathbf{e}_2$	$^1A'$	96(0), 135(0), 331(235), 631(28), 700(148), 794(132), 1304(174), 1743(364), 2260(867)
f	$^1A'$	48(63), 274(5), 471(2), 727(40), 772(23), 956(42), 1115(63), 1668(49), 2011(381)
$^3\mathbf{a}$	$^3A''$	210(6), 251(11), 378(39), 499(12), 623(0), 795(7), 926(32), 1317(21), 2304(1)
$^3\mathbf{d}$	$^3A''$	125(1), 199(2), 477(10), 555(18), 563(3), 757(61), 911(19), 1200(83), 2092(264)
$\mathbf{TSab}_1$		846*i*, 149, 374, 442, 547, 744, 1154, 1687, 2121
$\mathbf{TSb}_1\mathbf{b}_2$		173*i*, 136, 317, 536. 551, 598, 1143, 2059, 2249
$\mathbf{TSb}_2\mathbf{c}_1$	$^1A'$	356*i*, 428, 485, 627, 762, 1008, 1013, 1460, 1651
$\mathbf{TSc}_1\mathbf{c}_2$		202*i*, 136, 308, 350, 455, 579, 1011, 2032, 2117
$\mathbf{TSde}_1$		395*i*, 23, 515, 773, 783, 1023, 1068, 1345, 1800
$\mathbf{TSe}_1\mathbf{e}_2$		118*i*, 172, 358, 585, 665, 747, 1339, 1804, 2294
$\mathbf{TSe}_2\mathbf{f}$	$^1A'$	405*i*, 255, 429, 736, 754, 1076, 1227, 1359, 2131
$\mathbf{TSe}_1\mathbf{P}_3$	$^1A'$	508*i*, 86, 143, 319, 326, 495, 988, 1588, 2195
$\mathbf{TSe}_2\mathbf{P}_3$	$^1A'$	618*i*, 134, 156, 412, 633, 970, 1347, 1729, 2122
$\mathbf{TSfP}_4$	$^1A'$	154*i*, 272, 469, 725, 770, 944, 1119, 1676, 2012
$^3\mathbf{TSaP}_1$		601*i*, 233, 307, 486, 527, 822, 846, 1448, 1884
$^3\mathbf{TSRP}_2$		628*i*, 36, 95, 115, 237, 303, 538, 1905, 1944

[a] For isomers, the infrared intensities (km/mol) are given in parentheses. [b] Experimental values from ref 27. [c] Experimental values from ref 40.

possess all real frequencies, whereas transition states possess one and only one imaginary frequency. The zero-point energy (ZPE) corrections are performed at the same level of theory. To yield more accurate energetic information, higher level single-point energy calculations are carried out at the CCSD(T)[35] level (coupled-cluster approach with single and double substitutions, including a perturbative estimate of connected triple substitutions) with 6-311+G(2df,2p)[32−36] basis set (CCSD(T)/6-311+G(2df,2p)) by using the B3LYP/6-311G(d,p) optimized geometries. To confirm that the transition states connect designated intermediates, intrinsic reaction coordinate (IRC) calculation is employed at the B3LYP/ 6-311G(d,p) level. Unless otherwise specified, the CCSD(T) single-point energies with zero-point energy (ZPE) corrections (simplified as CCSD(T)//B3LYP) are used in the following discussions.

TABLE 2: Relative Energies (kcal/mol) (with Inclusion of the B3LYP/6-311G(d,p) Zero-Point Energy (ZPE) Corrections) of Reactants, Products, Isomers, and Transition States at the B3LYP and CCSD(T) Levels[a]

species	B3LYP	CCSD(T)	expt[b]	theory[c]
R ($CN + NO_2$)	0.0	0.0		
$\mathbf{P}_1$ (NCO + NO)	−66.7	−63.5	−61.2	−63.9
$\mathbf{P}_2$ (CNO + NO)	−4.2	−0.8		3.7
$\mathbf{P}_3$ (N_2O + CO)	−117.6	−121.3	−118.8	−121.4
$\mathbf{P}_4$ ($N_2 + CO_2$)	−203.3	−208.4	−206.1	−209.7
a	−57.8	−60.1		−59.1
$\mathbf{b}_1$	−79.8	−78.4		−80.2
$\mathbf{b}_2$	−80.7	−79.9		−77.6
$\mathbf{c}_1$	−26.7	−26.0		
$\mathbf{c}_2$	−23.8	−22.6		
d	−29.5	−29.6		
$\mathbf{e}_1$	−101.5	−97.4		−97.1
$\mathbf{e}_2$	−97.2	−93.8		−93.4
f	−85.3	−90.5		−92.7
$^3\mathbf{a}$	*−8.6*	*−1.1*		
$^3\mathbf{d}$	*25.5*	*33.6*		
$\mathbf{TSab}_1$	−3.9	−6.5		−5.3
$\mathbf{TSb}_1\mathbf{b}_2$	−74.3	−73.6		
$\mathbf{TSb}_2\mathbf{c}_1$	−14.0	−16.7		
$\mathbf{TSc}_1\mathbf{c}_2$	−16.5	−16.2		
$\mathbf{TSde}_1$	6.8	3.0		
$\mathbf{TSe}_1\mathbf{e}_2$	−96.1	−92.9		−93.3
$\mathbf{TSe}_2\mathbf{f}$	−77.0	−79.4		−79.6
$\mathbf{TSe}_1\mathbf{P}_3$	−34.5	−38.7		−45.8
$\mathbf{TSe}_2\mathbf{P}_3$	−72.5	−70.9		−71.7
$\mathbf{TSfP}_4$	−85.5	−90.6		−93.0
$^3\mathbf{TSaP}_1$	*11.8*	*19.7*		
$^3\mathbf{TSRP}_2$	*46.9*	*59.5*		

[a] The numbers in italics are for triplet species. [b] Thermochemical data for this reaction as obtained from heats of formation for CN (ref 27) and NCO (ref 29) along with the thermochemical tables (ref 28). [c] Theoretical results, at CCSD(T)/TZ2P//MBPT(2)/6-31G(d) level from ref 38.

3. Results and Discussion

3.1. Singlet Potential Energy Surface. The optimized structures of stationary points with the available experimental[27,37] and theoretical data[38,39] are depicted in Figure 1. The electronic states and harmonic vibrational frequencies including available experimental data[27,40] are given in Table 1. Table 2 displays the relative energies including ZPE corrections of the stationary points with the available experimental[27−29] and theoretical[38] values for comparison. For our discussion easier, the energy of reactants **R** is set to be zero for reference. By means of the transition states and their connected isomers or products, a schematic potential energy surface (PES) of the CN + NO_2 reaction in singlet is plotted in Figure 2. The potential curves of the initial carbon-to-nitrogen and nitrogen-to-nitrogen approach between CN ($^2\Sigma$) and NO_2 ($^2A_1$) on the singlet PES are presented in Figures 3 and 4, respectively.

3.1.1. Initial Association. On the singlet PES, the attack of the C atom of CN ($^2\Sigma$) radical on NO_2 ($^2A_1$) molecule may have three possible ways, i.e., middle-N attack, end-O attack, and side-NO-π bonding attack. The middle-N attack is rather attractive to form adduct **a** $NCNO_2$ (C_{2v}, $^1A_1$) without any entrance barrier. To further confirm the nonbarrier of this process, the pointwise potential curve at the B3LYP/6-311G(d,p) level is calculated, and the result is shown in Figure 3. In the calculation, the optimization for the other geometric parameters is done for every fixed internal C−N bond length. It is obvious that this addition process is a barrierless association. It is noticed that further full optimization of the minimum with a C−N distance of 1.4 Å as presented in Figure 3 leads to adduct **a** at the B3LYP/6-311G(d,p) level. From Figure 3, we know

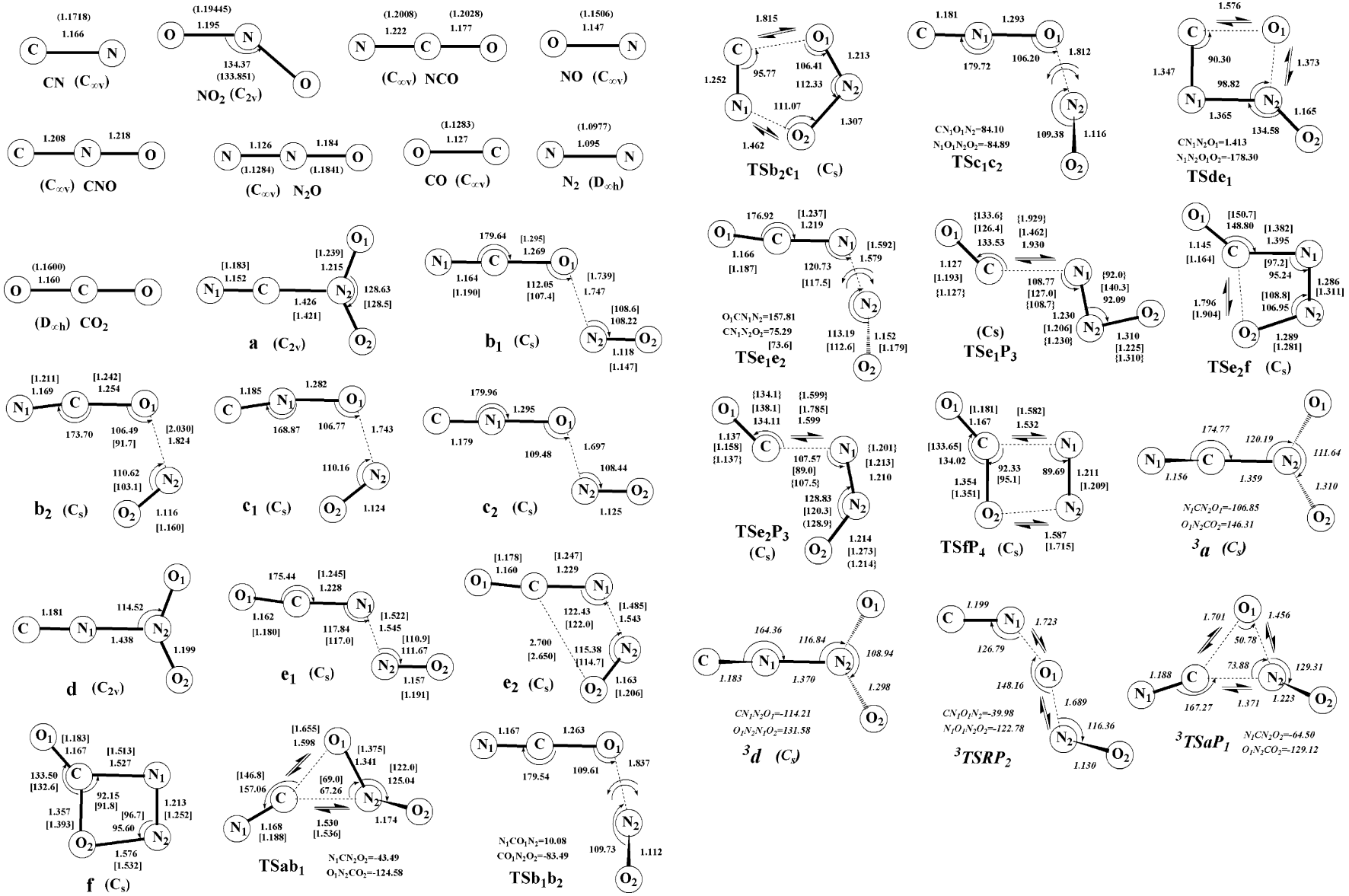

Figure 1. B3LYP/6-311G(d,p) optimized geometries of reactants, products, isomers, and transition states. The values in italics are for the triplet species. Bond distances are in angstroms and angles are in degrees. The values in "( )" are the experimental values (ref 37 for NO_2, NCO and ref 27 for CN, NO, N_2O, N_2, CO, CO_2). The values in "[ ]" are the theoretical results, at the MBPT(2)/6-31G(d) level from ref 38. The values in "{ }" are the theoretical results, at the B3LYP/6-311G(d,P) level from ref 39. In the transition states the direction of the imaginary frequency is indicated by "⇌".

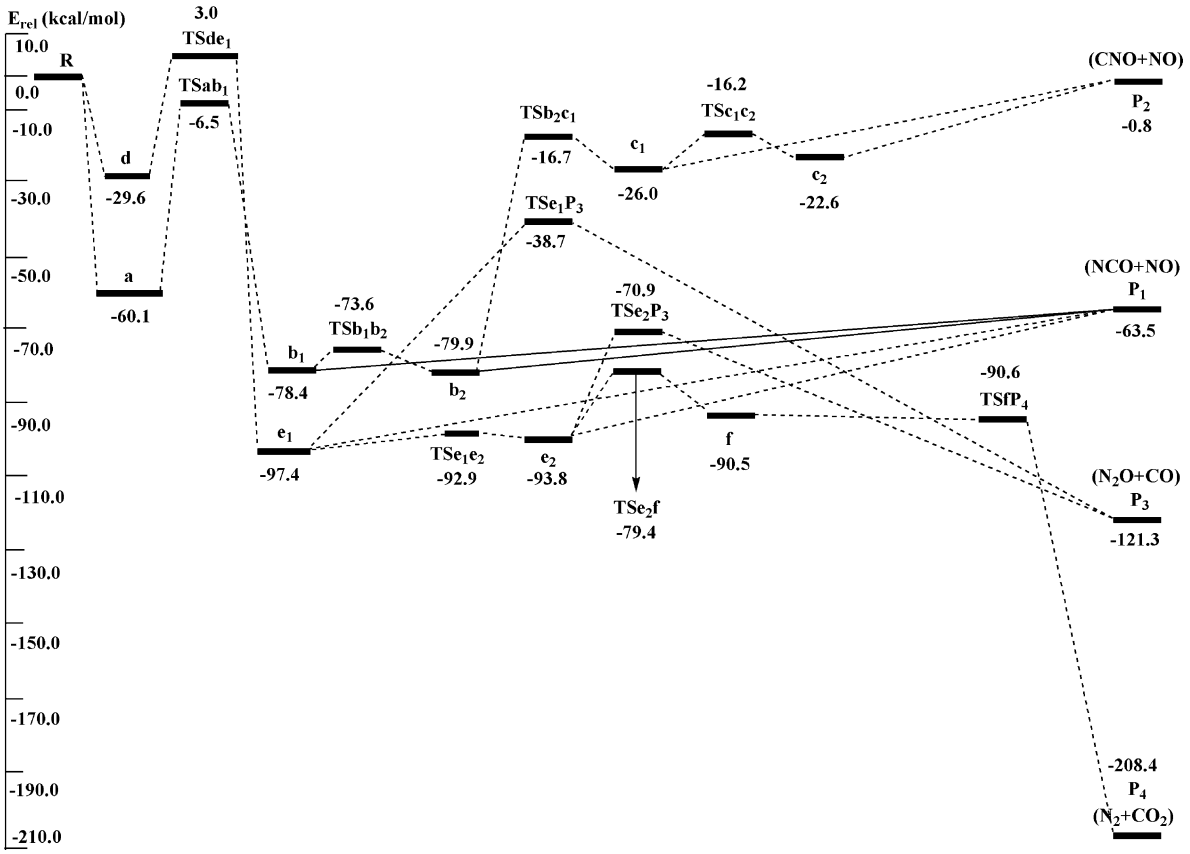

Figure 2. Schematic potential energy surface of the reaction channels for the CN + NO_2 reaction in singlet. Relative energies (E_{rel}, kcal/mol) are calculated at the CCSD(T) level.

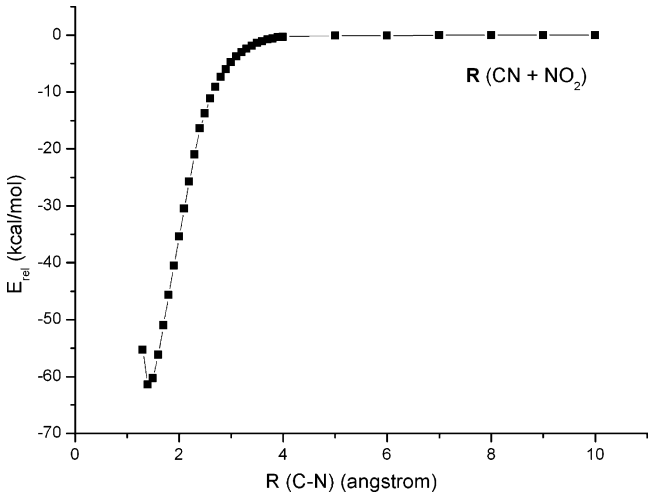

Figure 3. Relaxed potential energy curve for the formative process of the singlet adduct (**a**) for the CN + NO_2 reaction at the B3LYP/6-311G(d,p) level. *R* is the value of the C−N distance. E_{rel} is the relative energy (kcal/mol), with reference to the reactants **R** (CN + NO_2).

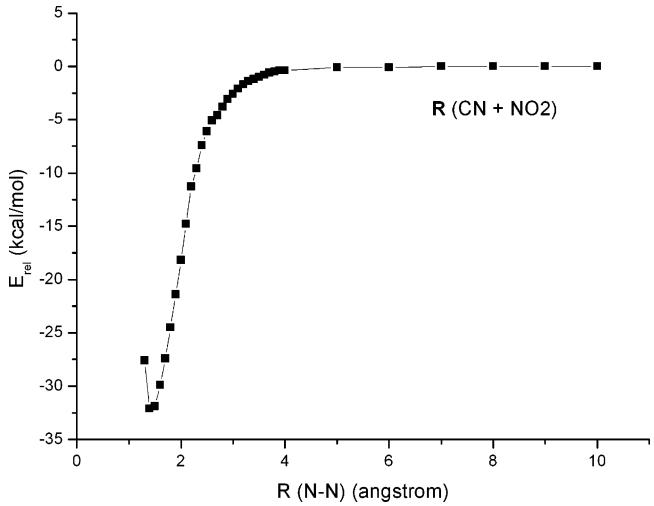

Figure 4. Relaxed potential energy curve for the formative process of the singlet adduct (**d**) for the CN + NO_2 reaction at the B3LYP/6-311G(d,p) level. *R* is the value of N−N distance. E_{rel} is the relative energy (kcal/mol), with reference to the reactants **R** (CN + NO_2).

that adduct **a** is formed as the C atom of CN approaches the N atom of NO_2 via an attractive potential energy surface. The binding energy of **a** with −60.1 kcal/mol indicates that this process makes adduct **a** highly activated, and this means that further isomerization or dissociation reactions can be promoted. The association is expected to be fast and will play a significant role in the reaction kinetics. We are unable to find the transition state for the end-O attack forming the weakly bound isomer **b** NCONO (C_s, $^1A'$) at the HF, B3LYP, and MP2 levels with 6-311G(d,p) or 6-31G(d,p) basis set. Yet, we expect that considerable barrier is needed to activate the short N═O double bond (1.195 Å) in NO_2 to form the much longer N−O weak bonds (1.747, 1.82 Å) in $\mathbf{b}_1$ and $\mathbf{b}_2$. Instead, $\mathbf{b}_1$ (trans-NCONO) can be barrierlessly formed from **R** via intermediate **a**, as shown in Figure 2. Optimization of the side-NO-π bonding attacking isomer usually leads to isomer **a** $NCNO_2$ or **b** NCONO. For the pathway of the N atom of CN ($^2\Sigma$) radical attacking on NO_2 ($^2A_1$), the nitrogen-to-nitrogen approach can barrierlessly lead to adduct **d** $CNNO_2$ (C_{2v}, $^1A_1$), as confirmed by the calculated pointwise potential curve for the formation of adduct **d** as plotted in Figure 4. The transition state for the nitrogen-to-oxygen approach forming the weakly bound isomer **c** CNONO (C_s, $^1A'$) cannot be located at the B3LYP/6-311G-

(d,p) level. However, the formation of isomer **c** is expected to be a barrier-consumed process since significant weakening of the short N═O double bond (1.195 Å) in NO_2 to form the long N−O weak bonds (1.743, 1.697 Å) in $\mathbf{c}_1$ and $\mathbf{c}_2$ is involved. Furthermore, either the isomer or transition state associated with the nitrogen-to-NO-π bonding attack are also not found at the same level. Searching for the nitrogen-to-NO-π bonding attacking isomer often leads to isomer **c** or **d**. Thus, on the singlet PES of the CN + NO_2 reaction, the exclusive feasible entrance channels are the barrierless carbon-to-nitrogen and nitrogen-to-nitrogen approaches to form adducts **a** $NCNO_2$ (C_{2v}, $^1A_1$) and **d** $CNNO_2$ (C_{2v}, $^1A_1$), respectively. Then, in the following discussions, we mainly discuss the formation pathways of various products starting from adduct **a** or **d**.

3.1.2. Stationary Points. Starting from the reactants **R** CN ($^2\Sigma$) + NO_2 ($^2A_1$), four energetically accessible primary products, $\mathbf{P}_1$ NCO($^2\Pi$) + NO($^2\Pi$), $\mathbf{P}_2$ CNO($^2\Pi$) + NO($^2\Pi$), $\mathbf{P}_3$ N_2O($^1\Sigma$) + CO($^1\Sigma$), and $\mathbf{P}_4$ N_2($^1\Sigma_g$) + CO_2($^1\Sigma_g$), are considered in the following sections, and these lie at −63.5, −0.8, −121.3, and −208.4 kcal/mol, respectively, at the CCSD-(T) level.

On the singlet PES of reaction CN + NO_2, two chainlike isomers **a** $NCNO_2$ (C_{2v}, $^1A_1$) and **d** $CNNO_2$ (C_{2v}, $^1A_1$), one cyclic isomer **f** c-NNOC−O (Cs, $^1A'$), and six weakly bound complex **b** ($\mathbf{b}_1$, $\mathbf{b}_2$) NCONO (C_s, $^1A'$), **c** ($\mathbf{c}_1$, c_2) CNONO (C_s, $^1A'$), and **e** ($\mathbf{e}_1$, e_2) OCNNO (C_s, $^1A'$) are located at the B3LYP/6-311G(d,p) level. Their relative energies (kcal/mol) are given in parentheses as follows: $\mathbf{e}_1$ (−97.4) < $\mathbf{e}_2$ (−93.8) < **f** (−90.5) < $\mathbf{b}_2$ (−79.9) < $\mathbf{b}_1$ (−78.4) < **a** (−60.1) < **d** (−29.6) < $\mathbf{c}_1$ (−26.0) < $\mathbf{c}_2$ (−22.6), with the linearly, weakly bound complex $\mathbf{e}_1$ (*trans*-OCNNO) as the global minimum. Isomers $\mathbf{b}_1$ and $\mathbf{b}_2$, $\mathbf{c}_1$ and $\mathbf{c}_2$, and $\mathbf{e}_1$ and $\mathbf{e}_2$ are three sets of cis−trans species for the NCONO, CNONO, and OCNNO structures, respectively. There exist very small barriers for interconversion between the cis−trans species. The barriers are 4.8, 6.3, 9.8, 6.4, 4.5, and 0.9 kcal/mol for $\mathbf{b}_1 \rightarrow \mathbf{b}_2$, $\mathbf{b}_2 \rightarrow \mathbf{b}_1$, $\mathbf{c}_1 \rightarrow \mathbf{c}_2$, $\mathbf{c}_2 \rightarrow \mathbf{c}_1$, $\mathbf{e}_1 \rightarrow \mathbf{e}_2$, and $\mathbf{e}_2 \rightarrow \mathbf{e}_1$ conversions, respectively. This is understandable since the N2−O2 bond just rotates along the long N2−O1 bond ($\mathbf{b}_1$, 1.747 Å; $\mathbf{b}_2$, 1.824 Å; $\mathbf{c}_1$, 1.743 Å; $\mathbf{c}_2$, 1.697 Å) or the long N−N bond ($\mathbf{e}_1$, 1.545 Å; $\mathbf{e}_2$, 1.543 Å).The easy interconversion between the cis−trans species indicates that they may coexist. To make clear the interrelation between various isomers or products, 10 transition states, i.e., $\mathbf{TSab}_1$ (C_1), $\mathbf{TSb}_1\mathbf{b}_2$ (C_1), $\mathbf{TSb}_2\mathbf{c}_1$ (C_s, $^1A'$), $\mathbf{TSc}_1\mathbf{c}_2$ (C_1), $\mathbf{TSde}_1$ (C_1), $\mathbf{TSe}_1\mathbf{e}_2$ (C_1), $\mathbf{TSe}_2\mathbf{f}$ (C_s, $^1A'$), $\mathbf{TSe}_1\mathbf{P}_3$ (C_s, $^1A'$), $\mathbf{TSe}_2\mathbf{P}_3$ (C_s, $^1A'$), and $\mathbf{TSfP}_4$ (C_s, $^1A'$), are obtained as shown in Figure 1. Notice that $\mathbf{TSab}_1$ is used to denote the transition state connecting isomers **a** and $\mathbf{b}_1$ as revealed by IRC calculations, and so on. For the $\mathbf{R} \rightarrow \mathbf{a}$, $\mathbf{R} \rightarrow \mathbf{d}$, $\mathbf{P}_1 \rightarrow \mathbf{b}_1$, $\mathbf{P}_1 \rightarrow \mathbf{b}_2$, $\mathbf{P}_1 \rightarrow \mathbf{e}_1$, $\mathbf{P}_1 \rightarrow \mathbf{e}_2$, $\mathbf{P}_2 \rightarrow \mathbf{c}_1$, and $\mathbf{P}_2 \rightarrow \mathbf{c}_2$ association processes that essentially result in only single-bond or weak-bond formation, no activation barrier is found in our calculations.

On the basis of the schematic PES presented in Figure 2, we can discuss the stability of various singlet $CNNO_2$ isomers toward isomerization and dissociation. For example, the most low-lying isomer $\mathbf{e}_1$ may isomerize to **d** via the four-centered transition state $\mathbf{TSde}_1$ or directly dissociate to $\mathbf{P}_1$, or lead to $\mathbf{P}_3$ via $\mathbf{TSe}_1\mathbf{P}_3$ with the potential barriers of 100.4, 33.9, and 58.7 kcal/mol at the CCSD(T)//B3LYP level for the three processes $\mathbf{e}_1 \rightarrow \mathbf{d}$, $\mathbf{e}_1 \rightarrow P_1$, and $\mathbf{e}_1 \rightarrow \mathbf{P}_3$, respectively. Thus, the $\mathbf{e}_1 \rightarrow \mathbf{P}_1$ dissociation with the barrier of 33.9 kcal/mol governs the kinetic stability of isomer $\mathbf{e}_1$. The kinetic stabilities of other isomers may be determined in the same way and given as follows (kcal/mol): **a** (53.6, $\mathbf{a} \rightarrow \mathbf{b}_1$) > $\mathbf{e}_1$ (33.9, $\mathbf{e}_1 \rightarrow \mathbf{P}_1$) > **d** (29.6, $\mathbf{d} \rightarrow \mathbf{R}$) > $\mathbf{c}_2$ (21.8, $\mathbf{c}_2 \rightarrow \mathbf{P}_2$) > $\mathbf{b}_2$ (16.4, $\mathbf{b}_2 \rightarrow \mathbf{P}_1$) > $\mathbf{b}_1$ (14.9, $\mathbf{b}_1 \rightarrow \mathbf{P}_1$) > $\mathbf{e}_2$ (14.4, $\mathbf{e}_2 \rightarrow \mathbf{f}$) > $\mathbf{c}_1$ (9.3, $\mathbf{c}_1 \rightarrow \mathbf{b}_2$) > **f** (−0.1, $\mathbf{f} \rightarrow \mathbf{P}_4$), with isomer **a** $NCNO_2$ to be the most stable. It should be noted that the negative conversion barrier for $\mathbf{f} \rightarrow \mathbf{P}_4$ is due to the inclusion of ZPE. This may indicate that intermediate **f** is kinetically unstable toward dissociation to product $\mathbf{P}_4$.

As shown in Figure 1 and Table 1, our calculated geometries and frequencies for the reactants and products agree very well with experimental values within 3%. For isomers and transition states, our B3LYP/6-311g(d,p) geometries are very close to recent MBPT(2)/6-31G(d) values[38] expect for $\mathbf{TSe}_1\mathbf{P}_3$ and $\mathbf{TSe}_2\mathbf{P}_3$. The large bond distance deviation in parentheses lies in the C−N1 bonding of $\mathbf{TSe}_1\mathbf{P}_3$ (0.468 Å) and $\mathbf{TSe}_2\mathbf{P}_3$ (0.168 Å). The large bond angle deviation lies in $\mathbf{TSe}_1\mathbf{P}_3$ (48.21°) and $\mathbf{TSe}_2\mathbf{P}_3$ (18.57°). Yet, our optimized geometries for $\mathbf{TSe}_1\mathbf{P}_3$ and $\mathbf{TSe}_2\mathbf{P}_3$ are consistent with the B3LYP/6-311G(d,p) values[39] within 0.01 Å and 0.1° for bond distance and angle, respectively. Most importantly, as listed in Table 2, there is good agreement between our calculated relative energies and the experimentally determined reaction heats of various products[27−29] with the largest deviation of 4% at the CCSD(T) level and 9% at the B3LYP level, respectively. It is known that the B3LYP method has been found to underestimate systematically the barrier heights.[41] Thus, in the present study, the energies are improved at the highly correlated CCSD(T) level. Moreover, our CCSD-(T)//B3LYP relative energies and recent CCSD(T)/ TZ2P//MBPT(2)/6-31G(d) values[38] are very close to each other except for product $\mathbf{P}_2$ (CNO + NO) and transition state $\mathbf{TSe}_1\mathbf{P}_3$ with the large discrepancies of 4.5 and 7.1 kcal/mol, respectively. However, such discrepancies will not affect our discussions on the reaction mechanism.

3.1.3. Isomerization and Dissociation Pathways. 3.1.3.1. Starting from Adduct **a**. The initial adduct **a** ($NCNO_2$) is a stable and branched chainlike isomer with C_{2v} symmetry and 60.1 kcal/mol energy below the reactants. As shown in Figure 2, the C−N2 bond rupture along with C−O1 bond formation of **a** may proceed to a C_s-symmetried weakly bound isomer $\mathbf{b}_1$ (*trans*-NCONO) with $^1A'$ electronic state via transition state $\mathbf{TSab}_1$ with the barrier of 53.6 kcal/mol. As seen in Figure 1, the C_1-symmetried $\mathbf{TSab}_1$ has a tight CN2O1 three-membered ring structure, in which the forming C−O1 bond length is 1.598 Å, while the breaking C−N2 bond length is 1.530 Å. The vibration mode of the imaginary frequency of $\mathbf{TSab}_1$ corresponds to C−N2 and C−O1 bonds stretch vibrations. Isomer **b** ($\mathbf{b}_1$, $\mathbf{b}_2$) then can easily lead to product $\mathbf{P}_1$ (CO_2 + CNO) via direct rupture of a long O1−N2 weak bond (1.747 Å in $\mathbf{b}_1$, 1.824 Å in $\mathbf{b}_2$). Only 14.9 and 16.4 kcal/mol barriers are needed to overcome for the processes $\mathbf{b}_1 \rightarrow \mathbf{P}_1$ and $\mathbf{b}_2 \rightarrow \mathbf{P}_1$, respectively. Such a multistep process can be described as

path 1 $\mathbf{P}_1$: $\mathbf{R} \rightarrow \mathbf{a} \rightarrow \mathbf{b}_1$ ($\mathbf{b}_2$) $\rightarrow \mathbf{P}_1$ (NCO + NO)

The isomer $\mathbf{b}_2$ (*cis*-NCONO) can alternatively undergo C−O1 bond cleavage associated with N1−O2 bond formation via transition state $\mathbf{TSb}_2\mathbf{c}_1$ to give the C_s-symmetried weak-bond isomer $\mathbf{c}_1$ (*cis*-CNONO), which can easily convert to $\mathbf{c}_2$ (*trans*-CNONO), followed by direct O1−N2 weak-bond (1.743 Å in $\mathbf{c}_1$, 1.697 Å in $\mathbf{c}_2$) fission to $\mathbf{P}_2$ (CNO + NO). The dissociation barriers are 25.2 and 21.8 kcal/mol for $\mathbf{c}_1 \rightarrow \mathbf{P}_2$ and $\mathbf{c}_2 \rightarrow \mathbf{P}_2$, respectively. $\mathbf{TSb}_2\mathbf{c}_1$ surmounts a high barrier of 63.2 kcal/mol, entering a relatively shallow potential well. It has a planar N1CO1N2O2 five-membered ring structure with $^1A'$ electronic state. The forming N1−O2 length is 1.462 Å, while the breaking C−O1 distance is relatively long with 1.815 Å. The imaginary frequency of 356*i* cm^{-1} mainly involves the simultaneous stretch

vibrations of N1−O2 and C−O1 bonds. The formation pathway of $\mathbf{P_2}$ is

path $\mathbf{P}_2$: $\mathbf{R} \rightarrow \mathbf{a} \rightarrow \mathbf{b}_1 \rightarrow \mathbf{b}_2 \rightarrow \mathbf{c}_1\ (\mathbf{c}_2) \rightarrow \mathbf{P}_2\ (\mathrm{CNO} + \mathrm{NO})$

3.1.3.2. Starting from Adduct **d**. The initially formed nitrogen-to-nitrogen approaching adduct **d** $CNNO_2$ (C_{2v}, $^1A_1$) has branched chainlike structure similar to adduct **a** $NCNO_2$ (C_{2v}, $^1A_1$), but lies 30.5 kcal/mol higher than **a**. The adduct **d** can isomerize to **a** C_s-symmetrized weak-bound isomer $\mathbf{e}_1$ (trans-OCNNO) with $^1A'$ electronic state via 1,3-O shift from N2 to C atom (i.e., $\mathbf{TSde}_1$) with a barrier of 32.6 kcal/mol. The nonplanar CN1N2O1 four-membered ring structure is found in $\mathbf{TSde}_1$. The vibration mode of imaginary frequency 395*i* cm^{-1} corresponds to C−O1 and N2−O1 bonds stretch vibrations. The migrating oxygen is 1.373 Å away from the origin (N2 atom) and 1.576 Å away from the migrating terminus (C atom). It should be pointed out that the process from $\mathbf{d} \rightarrow \mathbf{e}_1$ is kinetically less feasible at normal temperatures due to the high-energy transition state $\mathbf{TSde}_1$ above the reactants. However, since the $\mathbf{d} \rightarrow e_1$ conversion barrier is just 3.0 kcal/mol above the reactants, the conversion may become feasible at high temperatures. Subsequently, isomers **e** ($\mathbf{e}_1$, $\mathbf{e}_2$) can either directly dissociate to product $\mathbf{P}_1$ (NCO + NO) through the long N−N weak-bond (1.545 Å in $\mathbf{e}_1$, 1.543 Å in $\mathbf{e_2}$) cleavage or take a C−N1 bond rupture via transition state $\mathbf{TSe}_1\mathbf{P}_3$ or $\mathbf{TSe}_2\mathbf{P}_3$ leading to product $\mathbf{P}_3$ (N_2O + CO). Both $\mathbf{TSe}_1\mathbf{P}_3$ and $\mathbf{TSe}_2\mathbf{P}_3$ are of C_s symmetry with $^1A'$ electronic states. The chainlike structures of $\mathbf{TSe}_1\mathbf{P}_3$ and $\mathbf{TSe}_2\mathbf{P}_3$ are characterized by a markedly elongated C−N1 bond (1.930 Å in $\mathbf{TSe}_1\mathbf{P}_3$ and 1.599 Å in $\mathbf{TSe}_2\mathbf{P}_3$) and a compressed N1−N2 bond (1.230 Å in $\mathbf{TSe}_1\mathbf{P}_3$ and 1.210 Å in $\mathbf{TSe}_2\mathbf{P}_3$). The analysis of the two transition structures indicates that the vibrationally cold CO and N_2O can be formed. The imaginary frequencies of respective 508*i* and 618*i* cm^{-1} are relative to the stretch vibration of the C−N1 bond. These processes can simply be written as

path 2 $\mathbf{P}_1$: $\mathbf{R} \rightarrow \mathbf{d} \rightarrow \mathbf{e_1}\ (\mathbf{e_2}) \rightarrow \mathbf{P_1}\ (\mathrm{NCO} + \mathrm{NO})$

path $\mathbf{P}_3$: $\mathbf{R} \rightarrow \mathbf{d} \rightarrow \mathbf{e}_1\ (\mathbf{e}_2) \rightarrow \mathbf{P}_3\ (N_2O + CO)$

In addition, the closure of C and O2 atoms in isomer $\mathbf{e}_2$ (*cis*-OCNNO) via transition state $\mathbf{TSe}_2\mathbf{f}$ can form a planar four-membered ring intermediate **f** (c-NNOC−O) with the $^1A'$ state followed by its side N_2-elimination through $\mathbf{TSfP}_4$ to product $\mathbf{P}_4$ (N_2 + CO_2). The pathway leading to $\mathbf{P}_4$ can be depicted as

path $\mathbf{P}_4$: $\mathbf{R} \rightarrow \mathbf{d} \rightarrow \mathbf{e}_1 \rightarrow \mathbf{e}_2 \rightarrow \mathbf{f} \rightarrow \mathbf{P}_4\ (N_2 + CO_2)$

$\mathbf{TSe}_2\mathbf{f}$ and $\mathbf{TSfP}_4$ both involve a planar N1N2O2C four-membered ring structure with exocyclic CO1 bond and both of them have C_s symmetry and $^1A'$ electronic state. The forming C−O2 length in $\mathbf{TSe}_2\mathbf{f}$ is 1.796 Å, and the breaking C−N1 and O2−N2 distances in $\mathbf{TSfP}_4$ are 1.532 and 1.587 Å, respectively. The imaginary frequencies of respective 405*i* and 154*i* cm^{-1} indicate C−O2 bond breath vibration (in $\mathbf{TSe}_2\mathbf{f}$) and C−N1 and O2−N2 bonds stretch vibration (in $\mathbf{TSfP}_4$).

3.1.3.3. Reaction Mechanism and Experimental Implications. As can be seen from Figure 2, all the pathways (path 2 $\mathbf{P}_1$, path $\mathbf{P}_3$, and path $\mathbf{P}_4$) starting from initial adduct **d** involve the high-energy transition state $\mathbf{TSde}_1$, which lies 3.0 kcal/mol above **R** at the CCSD(T) level. While the isomers and transition states involved in the pathways (path 1 $\mathbf{P}_1$ and path $\mathbf{P}_2$) proceeded via initial adduct **a**, all lie below **R**. Therefore, path 2 $\mathbf{P_1}$, path $\mathbf{P}_3$, and path $\mathbf{P}_4$, leading to $\mathbf{P}_1$ (NCO + NO), $\mathbf{P}_3$ (N_2O + CO), and $\mathbf{P}_4$ (N_2 + CO_2), respectively, are much less competitive at normal temperatures than path 1 $\mathbf{P}_1$ and path $\mathbf{P}_2$, leading to respective $\mathbf{P}_1$ (NCO + NO) and $\mathbf{P}_2$ (CNO + NO), and may be of significance only at high temperatures. Thus, on the singlet PES of the CN + NO_2 reaction, path 1 $\mathbf{P}_1$ and path $\mathbf{P}_2$ dominate. With respect to these two pathways, path 1 $\mathbf{P}_1$ should be more feasible kinetically due to the less reaction steps and lower overall barrier from the common intermediate **b** to the final dissociation products. As a result, reflected in the final product distributions, we predict that (1) two products $\mathbf{P}_1$ (NCO + NO) and $\mathbf{P}_2$ (CNO + NO) may be observed, (2) $\mathbf{P}_1$ is the most favorable product, (3) $\mathbf{P}_2$ is the much less competitive product, and (4) formation of products $\mathbf{P}_3$ (N_2O + CO) and $\mathbf{P}_4$ (N_2 + CO_2) may become possible only at high temperatures.

In Wang et al.'s study,[7] they proposed that the CN + NO_2 reaction occurs by simple abstraction mechanism leading to product NCO + NO. Yet, on the basis of our present calculations, we think this reaction proceeds through a multistep process of association, isomerization, and dissociation as described by path 1 $\mathbf{P}_1$. Because all the isomers and transition states involved in this pathway lie below the reactants **R**, the CN + NO_2 reaction may proceed rapidly. This is confirmed by Wang et al.'s experiment.[7] Clearly, such a fast reaction may efficiently consume NO_2 emitted in the combustion processes. So, the title reaction is expected to play an important role in the NO_x formation and reducing processes.

Recently, a detailed theoretical investigation on the similar reaction of CN + O_2 was carried out.[42] By comparing the calculated results of the two reactions CN + NO_2 and CN + O_2, we found that (1) the attack of NO_2 and O_2 on CN radical both focus on the C-site, just in accordance with the dominant spin density on the carbon (0.828) rather than oxygen (0.172) atom within CN radical; (2) the initial association of these two reactions are both a barrierless addition process to form respective adducts $NCNO_2$ and NCO_2; (3) instead of simple abstraction mechanism, both reactions proceed through the complicated processes of association and dissociation; and (4) the two reactions are expected to be fast due to all of the transition states and isomers in the feasible pathways lying below the reactants **R**, as is confirmed by experiment.[7,43] The theoretical results presented here are expected to provide a useful basis for future investigation on other analogous cyanogen reactions.

3.2. Triplet Potential Energy Surface. On the triplet PES of the CN + NO_2 reaction, the carbon-to-nitrogen attacking isomer $^3\mathbf{a}$ ($NCNO_2$) is located. While the relative energy (−1.1 kcal/mol) of this triplet species $^3\mathbf{a}$ is 59 kcal/mol higher than that (−60.1 kcal/mol) of the singlet species **a**. Therefore, $^3\mathbf{a}$ is thermodynamically much less favorable than **a**. It should be noted that the attempt to obtain the transition state from **R** to $^3\mathbf{a}$ failed. Although $^3\mathbf{a}$ can further dissociate to product $\mathbf{P}_1$ (NCO + NO) via a concerted 1,2-O-shift along with C−N bond rupture, the involved high-lying transition state $^3\mathbf{TSaP}_1$, which lies 19.7 kcal/mol above **R**, effectively blocks the reaction CN + NO_2 to go through this triplet pathway. The nitrogen-to-nitrogen attacking isomer $^3\mathbf{d}$ ($CNNO_2$) is also located on the triplet PES, while it is 33.6 kcal/mol higher than **R** in energy. Therefore, formation of $^3\mathbf{d}$ is thermodynamically almost prohibited. Furthermore, the nitrogen-to-oxygen attack between CN and NO_2 can be realized via $^3\mathbf{TSRP}_2$ with a substantial barrier of 59.5 kcal/mol leading to product $\mathbf{P}_2$ (CNO + NO). In view of the much higher barriers involved in these processes, the triplet pathways may contribute less to the CN + NO_2 reaction compared with the singlet pathways, and thus will not be further discussed. Note that the optimized structures and corresponding

energies of the relevant isomers and transition states in triplet are also included in Figure 1 and Table 2 for comparison, with the numbers in italics.

4. Conclusions

A detailed singlet potential energy surface of the CN + NO_2 reaction system has been characterized at the B3LYP and CCSD(T) (single-point) levels. The mechanism can generally be summarized as association, isomerization, and dissociation processes. (1) This reaction is most likely initiated by the carbon-to-nitrogen approach to form adduct **a** ($NCNO_2$) with no barrier. Although nitrogen-to-nitrogen approach can barrierlessly lead to adduct **d** ($CNNO_2$), the high-lying transition state $\mathbf{TSde}_1$ (3.0 kcal/mol) effectively block **d** to go through the subsequent pathways at normal temperatures. (2) Two kinds of products $\mathbf{P}_1$ (NCO + NO) and $\mathbf{P}_2$ (CNO + NO) should be observed, in which $\mathbf{P}_1$ is the most favorable product, whereas $\mathbf{P}_2$ is the much less competitive product. Formation of $\mathbf{P}_3$ (N_2O + CO) and $\mathbf{P}_4$ (N_2 + CO_2) may become kinetically feasible at high temperatures. Since all the isomers and transition states involved in the dominant decomposition pathway (path 1 $\mathbf{P}_1$) are lower than the reactants **R** in energy, the CN + NO_2 reaction is expected to be fast, as is confirmed by experiment. So the CN + NO_2 reaction may be an efficient strategy for the decrease of NO_2 in atmosphere. The triplet pathways have much less competitive abilities and can be thus neglected.

This study can provide useful information for further experimental investigation on the title reaction and is expected to be helpful for understanding the combustion chemistry of nitrogen-containing compounds.

Acknowledgment. This work is supported by the National Natural Science Foundation of China (Grants 20333050, 20303007), the Doctor Foundation by the Ministry of Education, the Foundation for University Key Teacher by the Ministry of Education, the Key Subject of Science and Technology by the Ministry of Education of China, and the Key subject of Science and Technology by Jilin Province.

References and Notes

(1) Haynes, B. S.; Iverach, D.; Kirov, N. Y. *Fifteenth Symposium (International) on Combustion*; The Combustion Institute: Pittsburgh, PA, 1974; p 1103.

(2) Albers, E. A.; Hoyermann, K.; Schake, H.; Schmatijko, K. J.; Wagner, H. Gg.; Wolfrum, J. *Fifteenth Symposium (International) on Combustion*; The Combustion Institute: Pittsburgh, PA, 1974; p 765.

(3) Haynes, B. S. *Combust. Flame* **1977**, *28*, 113.

(4) Miller, J. A.; Branch, M. C.; Mclean, W. J.; Chandler, D. W.; Smooke, M. D.; Kee, R. J. *Twentieth Symposium (International) on Combustion*; The Combustion Institute: Pittsburgh, PA, 1984; p 673.

(5) Thorne, L. R.; Melius, C. F. Proceedings of the 26th JANNAF Combustion Meeting; also the 23rd Symposium (International) on Combustion, 1990.

(6) Yang, D. L.; Yu, T.; Lin, M. C.; Melius, C. F. *J. Chem. Phys.* **1992**, *97*, 222.

(7) Wang, N. S.; Yang, D. L.; Lin, M. C. *Chem. Phys. Lett.* **1989**, *163*, 479.

(8) Wang, N. S.; Yang, D. L.; Lin, M. C.; Melius, C. F. *Int. J. Chem. Kinet.* **1991**, *23*, 151.

(9) Balla, R. J.; Casleton, K. H.; Adams, J. S.; Pasternack, L. *J. Phys. Chem.* **1991**, *95*, 8694.

(10) Reisler, H.; Mangir, M.; Wittig, C. *Chem. Phys.* **1980**, *47*, 49.

(11) Miller, J. A.; Bowman, C. T. *Prog. Energy Combust. Sci.* **1989**, *15*, 287.

(12) Miller, J. A.; Bowman, C. T. *Int. J. Chem. Kinet.* **1991**, *23*, 289.

(13) Melius, C. F. *Proceedings of the 25th JaNaF Combustion Meeting*; CPIA Publication 498, Vol. 2; 1988; p 155.

(14) Ermolin, N. E.; Korobeinichev, O. P.; Kuibida, L. V.; Fomin, V. M.; Fiz. *Goreniya Vzryva* **1986**, *22*, 54.

(15) Baren, R. E.; Erickson, M. A.; Hershberger, J. F. *Int. J. Chem. Kinet.* **2002**, *34*, 12.

(16) Rim, K. T.; Hershberger, J. F. *J. Phys. Chem. A* **1998**, *102*, 4592.

(17) (a) Lanier, W. S.; Mulholland, J. A.; Beard, J. T. *Symp. (Int.) Combust. [Proc.]* **1988**, *21*, 1171. (b) Chen, S. L.; McCarthy. J. M.; Clark, W. D.; Heap, M. P.; Seeker, W. R.; Pershing, D. W. *Symp. (Int.) Combust. [Proc.]* **1988**, *21*, 1159.

(18) Myerson, A. L. *15th Symposium (International) on Combustion*; The Combustion Institute: Pittsburgh, PA, 1975; p 1085.

(19) Song, Y. H.; Blair, D. W.; Siminski, V. J.; Bartok, W. *18th Symposium (International) on Combustion*; The Combustion Institute: Pittsburgh, PA, 1981; p 53.

(20) Chen, S. L.; McCarthy, J. M.; Clark, W. D.; Heap. M. P.; Seeker, W. R.; Pershing,D. W. *21st Symposium (International) on Combustion*; The Combustion Institute: Pittsburgh, PA, 1986; p 1159.

(21) Yamada, F.; Slagle, I. R.; Gutman, D. *Chem. Phys. Lett.* **1981**, *83*, 409.

(22) Zhang, J. X.; Liu, J. Y.; Li, Z. S.; Sun, C. C. *J. Comput. Chem.* **2005**, *26*, 807.

(23) Thweatt, W. D.; Erickson, M. A.; Hershberger, J. F. *J. Phys. Chem. A* **2004**, *108*, 74.

(24) Zhang, J. X.; Liu, J. Y.; Li, Z. S.; Sun, C. C. *J. Phys. Chem. A*, in press.

(25) Carl, S. A.; Sun, Q.; Teugels, L.; Peeters, J. *Phys. Chem. Chem. Phys.* **2003**, *5*, 5424.

(26) Zhang, J. X.; Li, Z. S.; Liu, J. Y.; Sun, C. C. *J. Chem. Phys.*, submitted for publication.

(27) Lide, D. R., Ed. *CRC Handbook of Chemistry and Physics*, 80th ed.; CRC Press: Boca Raton, FL, 1999.

(28) Chase, M. W., Jr.; et al. JANAF Thermochemical Tables, 3rd ed. *J. Phys. Chem. Ref. Data* **1985**, **14** (Suppl. 1).

(29) Cyr, D. R.; Continetti, R. E.; Meta, R. B.; Osborn, D. L.; Neumark, D. M. *J. Chem. Phys.* **1992**, *97*, 4937.

(30) Frisch, M. J.; Trucks, G. W.; Schlegel, H. B.; Scuseria, G. E.; Robb, M. A.; Cheeseman, J. R.; Zakrzewski, V. G.; Montgomery, J. A.; Stratmann, R. E.; Burant, J. C.; Dapprich, S.; Millam, J. M.; Daniels, A. D.; Kudin, K. N.; Strain, M. C.; Farkas, O.; Tomasi, J.; Barone, V.; Cossi, M.; Cammi, R.; Mennucci, B.; Pomelli, C.; Adamo, C.; Clifford, S.; Ochterski, J.; Petersson, G. A.; Ayala, P. Y.; Cui, Q.; Morokuma, K.; Malick, D. K.; Rabuck, A. D.; Raghavachari, K.; Foresman, J. B.; Cioslowski, J.; Oritz, J. Gomperts, R.; Martin, R. L.; Fox, D. J.; Keith, T.; Al-Lanham, M. A.; Peng, Johnson, B. G.; Chen, W.; Wong, M. W.; Andres, J. L.; Head-Gordon, M.; Replogle, E. S.; Pople, J. A. *Gaussian 98*, revision A.9; Gaussian, Inc.: Pittsburgh, PA, 1998.

(31) Becke, A. D. *J. Chem. Phys.* **1993**, *98*, 5648.

(32) McLean, A. D.; Chandler, G. S. *J. Chem. Phys.* **1980**, *72*, 5639.

(33) Krishnan, R.; Binkley, J. S.; Seeger, R.; Pople, J. A. *J. Chem. Phys.* **1980**, *72*, 650.

(34) Frisch, M. J.; Pople, J. A.; Binkley, J. S. Self-Consistent Molecular Orbital Methods 25: Supplementary Functions for Gaussian Basis Sets. *J. Chem. Phys.* **1984**, *80*, 3265.

(35) Pople, J. A.; Head-Gordon, M.; Raghavachari, K. J. *J. Chem. Phys.* **1987**, *87*, 5968.

(36) Clark, T.; Chandrasekhar, J.; Spitznagel, G. W.; Schleyer, P. v. R. *J. Comput. Chem.* **1983**, *4*, 294.

(37) Kuchitsu, K. Structure of Free Polyatomic Molecules Basic Data, 1998.

(38) Korkin, A. A.; Leszczynski, J.; Bartlett, R. J. *J. Phys. Chem.* **1996**, *100*, 19840.

(39) Zhu, R.; Lin, M. C. *J. Phys. Chem. A* **2000**, *104*, 10807.

(40) NIST Chemistry WebBook, NIST Standard Reference database Number 69, March 2003 Release. Vibrational frequency data compiled by M. E. Jacox.

(41) Lynch, J.; Fast, P. L.; Harris, M.; Truhlar, D. G. *J. Phys. Chem. A* **2000**, *104*, 4811.

(42) Ou, Z. W.; Zhu, H.; Li, Z. S.; Zhang, X. K.; Zhang, Q. Y. *Chem. Phys. Lett.* **2002**, *353*, 304.

(43) (a) Atakan, B.; Wolfrum, J. *Chem. Phys. Lett.* **1991**, *178*, 157. (b) Balla, R. J.; Casleton, K. H. *J. Phys. Chem.* **1991**, *95*, 2344.